Biochemistry **2000,** *39,* 14025−14039

NMR Studies of the Association of Cytochrome b_5 with Cytochrome c[†]

Kellie Hom, Qi-Feng Ma, Gary Wolfe, Hong Zhang, Elizabeth M. Storch,[‡] Valerie Daggett,*[,§]
Vladimir J. Basus,[‡] and Lucy Waskell*[,§]

*Department of Pharmaceutical Chemistry, University of California, San Francisco, California 94143, and
Department of Anesthesia, University of Michigan, Ann Arbor, Michigan, and the VA Medical Center, 2215 Fuller Road,
Ann Arbor, Michigan 48105, and Department of Medicinal Chemistry, University of Washington,
Seattle, Washington, 98195-7610*

Received May 18, 2000; Revised Manuscript Received August 25, 2000

ABSTRACT: In an effort to gain greater insight into the molecular mechanism of the electron-transfer reactions of cytochrome b_5, the bovine cytochrome b_5−horse cytochrome *c* complex has been investigated by high-resolution multidimensional NMR spectroscopy using ^{13}C, ^{15}N-labeled cytochrome b_5 expressed from a synthetic gene. Chemical shifts of the backbone ^{15}N, ^{1}H, and ^{13}C resonances for 81 of the 82 residues of [U-90% ^{13}C,U-90% ^{15}N]-ferrous cytochrome b_5 in a 1:1 complex with ferrous cytochrome *c* were compared with those of ferrous cytochrome b_5 in the absence of cytochrome *c*. A total of 51% of these residues showed small, but significant, changes in chemical shifts (the largest shifts were 0.1 ppm for the amide ^{1}H, 1.15 for $^{13}C_{\alpha}$, 1.03 ppm for the amide ^{15}N, and 0.15 ppm for the $^{1}H_{\alpha}$ resonances). Some of the residues exhibiting chemical shift changes are located in a region that has been implicated as the binding surface to cyt *c* [Salemme, F. R. (1976) *J. Mol. Biol. 10*, 563−568]. Surprisingly, many of the residues with changes are not located on this surface. Instead, they are located within and around a cleft observed to form in a molecular dynamics study of cytochrome b_5 [Storch, E. M., and Daggett, V. (1995) *Biochemistry 34*, 9682−9693]. The rim of this cleft can readily accommodate cytochrome *c*. Molecular dynamics simulations of the Salemme and cleft complexes were performed for 2 ns and both complexes were stable.

The cytochrome b_5 (cyt b_5)−cytochrome *c* (cyt *c*)[1] electron-transfer complex has been the subject of numerous studies, including NMR spectroscopy (*1*) and molecular dynamics (MD) simulations (*2*). For a recent review, see ref *3*. The availability of high-resolution structures of each of the proteins, determined by crystallography (*4*, *5*) and more recently by NMR (*6*), as well as the relatively small sizes of the proteins, has made this complex an important model for the investigation of biological electron-transfer reactions.

A model of the cyt b_5−cyt *c* complex was proposed by Salemme (*7*). For this model, the crystal structures of the component proteins were docked using a least-squares fitting procedure to optimize the intermolecular interactions, surface packing and placement of the hemes. The key features in this static model of the complex include (1) a 1:1 binding stoichiometry in the complex; (2) four intermolecular complementary charge interactions (E48, E44, D60, the heme 6-propionate of cyt b_5 with K13, K27, K72, K79, respectively, of cyt c), where the separation between a lysine side-chain nitrogen and a carboxylic oxygen in the charge-pair is approximately 3 Å; (3) the heme prosthetic groups of the molecules are oriented in nearly the same plane with a tilt of approximately 15°; (4) bulk water is excluded at the interface. This model has provided a basis for development of experimental strategies to evaluate the mechanism by which cyt b_5 and cyt *c* bind and subsequently undergo an electron-transfer reaction. Cyt b_5 is the low potential protein and transfers an electron to cyt *c*. Although the general features of the Salemme model have been supported by subsequent experimental work (see below), as well as theoretical studies, such as molecular dynamics simulations (*2*) and Brownian dynamics simulations (*8*, *9*) a definitive identification of the inter-cytochrome binding surface has not been obtained.

Steady-state kinetic measurements indicate that complex formation and the subsequent transfer of an electron from cyt b_5 to cyt *c* is dependent on pH and ionic strength (*10*−*12*). At ionic strengths greater than 0.2 M, the reaction is bimolecular and therefore second order. The complex is maximally stable at pH 7, midway between the isoelectric points of the individual proteins. The binding between cyt b_5 and cyt *c* is largely entropy driven presumably due to extensive solvent reorganization upon complexation (*10*).

The productive electron-transfer complex forms from an unproductive orientation by a diffusion mechanism (*8*, *9*). Previous NMR studies of the cyt b_5−cyt *c* complex have supported the model proposed by Salemme (*7*, *13*, *14*, *15*,

---

[†] This work was supported by grants from the Veterans Administration Merit Review and the National Institutes of Health, GM 35533 to L.W., and the National Institutes of Health, GM 50789 to V.D.

* To whom correspondence should be addressed. Phone: (734) 769-7100 ext. 5858. Fax: (734) 213-6985. E-mail: (L.W.) Waskell@umich.edu, (V.D.) daggett@u.washington.edu.

[‡] Department of Pharmaceutical Chemistry.

[§] Department of Medicinal Chemistry.

[1] Abbreviations: cyt b_5, cytochrome b_5; cyt *c*, cytochrome *c*; MD, molecular dynamics; IPTG, isopropyl β-D-thiogalactopyranoside; apo b_5, apocytochrome b_5; C′, carbonyl carbon; FID, free-induction-decay; NOESY, nuclear Overhauser enhancement spectroscopy; HMQC, heteronuclear multiple quantum coherence; HSQC, heteronuclear single quantum coherence; TPPI, time proportional phase incrementation; TOCSY, total correlation spectroscopy.

10.1021/bi001129o CCC: $19.00

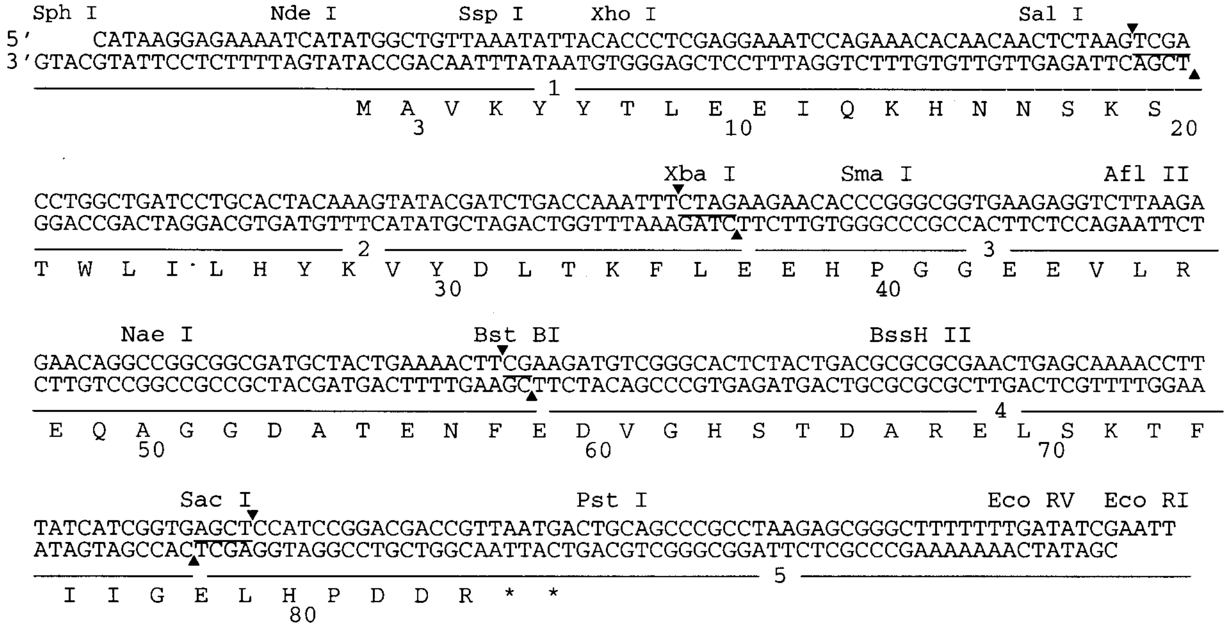

FIGURE 1: Nucleotide and amino acid sequence of the synthetic cytochrome b_5 gene. The five synthetic oligonucleotide fragments are underlined and numbered. The unique restriction sites are shown and the oligonucleotide boundaries are indicated by vertical lines. The stop codons are specified by asterisks.

1, *16*), but have not been of sufficiently high resolution to precisely define the interprotein binding surfaces. The binding stoichiometry of cyt b_5 and cyt *c* has been determined by optical difference spectroscopy (*10*) and NMR (*13*). Although one investigator has suggested a ternary complex between two molecules of cyt *c* and one of cyt b_5 (*15*, *17*), Mauk and co-workers (*3*) suggested that this ternary complex was the result of the use of nonuniform ionic strength and cyt *c* concentrations throughout the titration experiments, as well as phosphate ion, which was present at a relatively high and variable concentration.

In the experiments reported herein, an attempt has been made to identify and characterize in greater detail the binding interface between cyt b_5 and cyt *c*. The bovine cyt b_5 gene has been synthesized, and a ^{13}C-^{15}N labeled cyt b_5 has been purified from an *Escherichia coli* overexpression system. All proton, ^{13}C and ^{15}N, resonances have been assigned in cyt b_5, and the cyt b_5 residues whose chemical shifts change in the presence of cyt *c* have been identified. The results support Salemme's model (*7*), but intriguingly raise the possibility that cyt *c* may also bind in a cleft in cyt b_5 predicted by molecular dynamics (*18*).

MATERIALS AND METHODS

Unless specified otherwise, all restriction endonucleases and DNA-modifying enzymes were purchased from Gibco BRL and all chemicals were obtained from Sigma. The DNA sequencing kit and pUC 19 plasmid were from United States Biochemicals. ^{13}C, ^{15}N-labeled Celtone was from Martek, Columbia, MD, and ^{13}C-sodium acetate was from Cambridge Isotope Laboratory. Standard protocols for plasmid isolation, transformation, restriction endonuclease digestion and DNA ligation, as well as culture media preparations, were used unless stated otherwise (*19*). *E. coli* strains BL21(DE3) and BL21(DE3) pLysS were purchased from Novagen. *E. coli* JM109 was from Promega. Horse heart cyt *c* (Type IV) was purchased from Sigma and used without further purification.

Design and Synthesis of the Bovine Cyt b_5 Gene. The DNA sequence of our synthetic cyt b_5 gene was based on the cDNA sequence of the bovine cyt b_5 (*20*). To ensure maximum expression of the cyt b_5 gene, the codons most frequently used by *E. coli* were substituted for the codons in the natural bovine gene (*21*). Predicted stem loop structures with stems longer than four base pairs on the mRNA sequence were identified with the program Eugene and an effort was made to eliminate such structures in the final gene. The program Pincer was used to generate a restriction map of the gene. Eugene and Pincer are programs obtained from and used in Dr. Daniel Santi's laboratory, University of California, San Francisco. To facilitate synthesis and assembly of the gene, four unique restriction sites were encoded in the gene (Figure 1). The oligonucleotides were synthesized at the Biomolecular Resource Center, University of California, San Francisco. The complementary oligonucleotide pairs were individually purified on an 8% polyacrylamide/8 M urea gel, phosphorylated with polynucleotide kinase, and annealed to form a double-stranded DNA fragment. Each of the five oligonucleotide fragments was sequentially cloned into the pUC 19 vector beginning with fragment 5. The pUC 19 vector was cleaved in the polylinker region by the two restriction enzymes that corresponded to the two restriction sites flanking the double-stranded DNA fragment. The linearized vector was dephosphorylated with calf intestine phosphatase and ligated to one of the double-stranded DNA oligonucleotides. The vector containing the cyt b_5 oligonucleotide insert was then used to transform *E. coli* JM109. This amplified plasmid was then used as the vector for the insertion of the next cyt b_5 oligonucleotide. When all five fragments had been sequentially assembled into the pUC 19 vector, the resulting plasmid, pUC b_5, was sequenced by both the conventional dideoxy DNA sequencing method and by an automatic DNA sequencer (Applied Biosystems, model 373A) at the Biomolecular Resource Center at the University of California, San Francisco. The DNA and amino acid sequence of the synthetic cyt b_5 gene are illustrated in Figure 1. The gene is composed of a ribosome binding site, start and stop codons, a transcription terminator, and four unique restriction sites. It codes for the trypsin-solubilized form of bovine cytochrome b_5 from amino acids A3 to R84 according to the cyt b_5 numbering system used by Mathews and coworkers (4). In the nontrypsin treated native protein, A3 corresponds to A7 (*20*).

Expression, Purification, and Characterization of Cyt b_5. To obtain high levels of expression, the cyt b_5 gene was excised from pUC b_5 at the *Nde*/*Eco*R1 restriction sites and subcloned into the T7 expression vector pHB40P (gift of Dr. Daniel Santi, University of California, San Francisco). The resulting plasmid, pHB b_5 was used to transform *E. coli* strain BL21(DE3) and BL21(DE3) pLysS for the production of unlabeled and ^{13}C, ^{15}N-labeled cyt b_5, respectively. The transformed bacteria were then plated on plates prepared with LB medium containing 50 mg/L of ampicillin and incubated at 37 °C for 10 h. A single colony was inoculated into a 500 mL flask containing 100 mL of LB medium and ampicillin at 50 mg/L. The flask was incubated at 37 °C with shaking at 250 rpm until the absorbance at 600 nm was between 1.5 and 2 (approximately 8 h). IPTG (isopropyl β-D-thiogalactopyranoside) was added to a final concentration of 0.5 mM, and the cells were allowed to grow overnight for approximately 12 h under the same conditions. The culture was centrifuged at 5000 rpm in a JA-10 rotor to pellet the cells. Apocytochrome b_5 was found in the supernatant. Holo cyt b_5 was reconstituted by adding 2 mL of a solution of 1 mM hemin, 50% ethanol, and 0.1 N NaOH, to 100 mL of supernatant. Hemin was added in an approximately 1.5 molar excess over apocyt b_5. The supernatant containing the reconstituted holo cyt b_5 was dialyzed against 50 mM potassium phosphate buffer (pH 7.2) using Spectra/Por 3 dialysis tubing with a 3000 molecular weight cut off. The dialyzed supernatant was purified with minor modifications of the previously described procedure (*22*). The supernatant from 10 500 mL flasks was typically pooled and loaded onto a DE 52 cellulose column (Pharmacia) preequilibrated with the same phosphate buffer. A 3 × 20 cm column was used with a prep of 1 L of supernatant. The column was eluted with a linear gradient of 1 L phosphate buffer, pH 7.2, from 50 to 170 mM and the red colored fractions were pooled and concentrated to 2 mL using an Amicon Y3 membrane. The concentrated cyt b_5 was loaded onto a Sephadex G75 (Pharmacia) column (1.5 × 70 cm) preequilibrated with 100 mM Tris-HCl buffer, pH 7.6, at 25 °C and eluted with the same buffer. The fractions with an A413/A280 ratio greater than 5.9 were pooled, concentrated on an Amicon Y3 membrane and characterized. The cyt b_5 concentration of the purified protein was determined using an extinction coefficient of 117 mM^{-1} cm^{-1} at 412 nm (*23*). The spectrum of the expressed, purified protein was indistinguishable from that of an authentic sample of cyt b_5. The cyt b_5 ran as a single band on a 15% SDS−polyacrylamide gel and comigrated with an authentic sample of bovine cyt b_5. Electrospray mass spectrometry determined the molecular weight of the cyt b_5 to be 9460 ± 1, as expected. The concentration of cyt b_5 in the culture medium ranged from 120 to 213 mg/L.

Isolation and Characterization of the ^{13}*C*, ^{15}*N-labeled Cyt* b_5. To obtain the ^{13}C, ^{15}N-labeled cyt b_5, the plasmid pHB b_5 was expressed in BL21 (DE3) pLysS (pHB b_5 was not stable in BL21[DE3]). The *E. coli* were grown in the same manner as for the unlabeled protein, except that the bacteria were grown in a medium which contained ^{13}C, ^{15}N-labeled Celtone (a hydrolysate of ^{13}C, ^{15}N-labeled seaweed), 5 g/L; ^{13}C-labeled sodium acetate, 2 g/L; $FeCl_3$, 1 μM; $ZnSO_4$, 25 μM; $MnC1_2$, 3.9 μg/mL; $MgSO_4{\cdot}7H_2O$, 10 mg/mL; K_2HPO_4, 18 mg/mL; KH_2PO_4, 14 mg/mL; NaCl, 17 mM; thiamine, 5 μg/mL; and vitamin mix (biotin, choline chloride, folic acid, niacinamide, D-pentothanate, pyridoxal HCl, riboflavin), 0.5 μg/mL each. When the protein was expressed in the ^{13}C, ^{15}N-labeled Celtone, the expression of cyt b_5 was somewhat less at approximately 100 mg/L cell culture. The labeled protein was purified in the same manner as the unlabeled native protein. A total of 48 mg of pure protein was obtained from 450 mL cell culture which contained 5.2 g of ^{13}C,^{15}N-Celtone.

The extent of incorporation of ^{13}C and ^{15}N into cyt b_5 was determined by electrospray mass spectrometry. The average mass of the labeled cyt b_5 was 9966 ± 1.5 Da. The calculated mass for 100% incorporation of the two heavy isotopes is 10 014.3 Da and the mass of the native protein is 9482.4 Da. This means the average labeling of cyt b_5 is 90.9± 0.3%. A Fisons/VG (Manchester, U.K.) Bio-Q electrospray mass spectrometer, equipped with a Lab-Base data system, was used for the molecular weight determinations.

Quantitation of Cyt b_5 *Expression in the Culture Medium.* Due to the endogenous cytochromes present in *E. coli*, cyt b_5 was quantitated in the crude culture medium supernatant as previously described (*24*). Briefly, the supernatant containing the holo cyt b_5 was reduced in the sample cuvette with a few grains of sodium dithionite. The oxidized cyt b_5 was placed in the reference cuvette. The holo cyt b_5 content was calculated from the difference spectrum of the reduced minus oxidized cyt b_5 using a molar extinction coefficient of 185 mM^{-1} cm^{-1} for the absorbance difference at 425 minus that at 409 nm.

Sample Preparation. The unbound ferrous cyt b_5 sample contained 9 mM protein in 100 mM potassium phosphate at pH 6.5 and was prepared as follows. Cyt b_5 which had been lyophilized from a NH_4HCO_3 buffer was dissolved in 100 mM, pH 7, potassium phosphate buffer and the pH was adjusted to 6.5. The protein solution in the NMR tube was first purged with argon, and subsequently reduced by addition of a small aliquot of solid sodium dithionite; the NMR tube was sealed under vacuum with a gas-oxygen torch. After completion of the NMR experiments, the sealed NMR tube was opened and the pH was measured; it was 6.5. The 9 mM cyt b_5 sample was dialyzed thoroughly against 1 mM phosphate buffer (pH 7) or deionized water (pH 7) and then used for preparing additional samples: the ferric cyt b_5− cyt *c* complex, as well as the free ferric cyt b_5. The sample of the ferrous cyt b_5−ferrous cyt *c* complex (1 mM:1.2 mM) in 1 mM potassium phosphate was prepared from the original lyophilized cyt b_5 by adding 1.2 times the molar amount of solid cyt *c* to a 1 mM solution of cyt b_5 in 1 mM potassium phosphate. The pH of the protein complex was adjusted to 6.5 and reduced to the ferrous state as described above. After completion of the NMR experiments, the sealed tube was opened and the pH of the sample was determined to be 6.5.

For the pH titration study on ferric cyt b_5, a 1 mM sample in water was prepared from a concentrated solution of cyt b_5 in deionized water. The pH of the sample was first adjusted from 6.5 in approximately 0.5 pH unit steps toward the alkaline range and then lowered to the acidic range. To minimize the amount of salt formed during the course of pH adjustments, the sample at the alkaline pH extreme of 9.0, was dialyzed against water and then brought to the acidic range by adding small amounts of concentrated HCl. The ferric cyt b_5 sample was studied at pH 6.0, 6.5, 7.0, 7.6, 7.9, 8.4, and 9.0.

A solution of ferric cyt b_5−ferric cyt *c* (1 mM:1.2 mM) complex was prepared for pH titration study by combining appropriate amounts of concentrated cyt b_5 and cyt *c* solutions, both dialyzed against deionized water (pH 7), and adjusting the pH to appropriate values. The ferric cyt b_5−ferric cyt *c* complex was studied at pH 5.5, 6.1, 6.5, 7.0, 7.6, 8.0, and 8.4. A small precipitate was formed at pH 5.5, presumably due to the limited solubility of cyt b_5 near its isoelectric point (*25*). NMR spectra were obtained after the precipitate was removed by microcentrifugation. All pH adjustments were made with concentrated HCl or KOH. All samples contained 10% D_2O and appropriate amounts of trimethylsilylpropionic acid (TSP) as an internal chemical shift reference.

NMR Spectroscopy. All NMR experiments were performed at 25 °C, on a Varian Unity-plus 600 or a Varian Inova 600 MHz spectrometer, both equipped with a triple-resonance probe. Water suppression was accomplished with the use of pulsed-field gradients. The following 14 experiments were performed on free ferrous ^{13}C, ^{15}N-labeled cyt b_5: (1) ^{15}N-^{1}H refocused gradient-enhanced HSQC (*26*); (2) ^{13}C-^{1}H gradient-enhanced HSQC optimized for aromatic carbon (*27*); (3) (HB)CB(CGCD)(*28*); (4) (HB)CB(CGCDCE)HE (*28*); (5) ^{1}H-TOCSY-relayed ct-[^{13}C,^{1}H]-HMQC (*29*); (6) HNCO (*30*); (7) HNCA (31,32); (8) HNCACB (*33;30*); (9) CBCA(CO)NNH (*34*); (10) HBHA(CO)NNH (*35*); (11) HCCH-TOCSY (*36*); (12) ct-HCACO (*37*) and (12) a 2D version of the ct-HCACO experiment with t_1 evolution on C′; (13) ^{13}C-edited NOESY−HMQC (*30*); (14) ^{15}N-edited NOESY−HMQC (modified from the ^{13}C-edited NOESY−HMQC experiment above.

The following seven experiments were performed on the ferrous cyt b_5−ferrous cyt *c* complex: (1) ^{15}N-^{1}H refocused gradient-enhanced HSQC; (2) ^{13}C-^{1}H gradient-enhanced HSQC optimized for aromatic carbon; (3) HNCA; (4) HCCH-TOCSY; (5) 2D version of ct-HCACO with t_1 evolution on C′; (6) a 2D version of HNCOCA with t_1 evolution on C′ (*32*); (7) mq-HNCO (*38*).

For the pH titration studies on the free ferric cyt b_5 and ferric cyt b_5−ferric cyt *c* complex, ^{15}N-^{1}H refocused gradient-enhanced HSQC and ^{13}C-^{1}H gradient-enhanced HSQC optimized for aromatic carbon experiments were performed at each pH value. A 2D version of HNCOCA with t_1 evolution on C_α experiment was performed at selected pHs. To assign the resonances of cyt b_5 in both free and complexed forms in the ferric state, HNCA and HCCH-TOCSY spectra were obtained for both the free and bound samples.

Identical NMR spectrum acquisition parameters (given below) were used for both the free and complexed cyt b_5 in the two oxidation states, where applicable. The ^{1}H spectral width in the directly detected dimension for these experiments was 8000 Hz (reduced samples) and 10,000 Hz (oxidized samples). The proton spectral width was 5500 Hz in the indirectly detected dimension of HCCH-TOCSY and 5000 Hz for ^{1}H-TOCSY-relayed ct-[^{13}C,^{1}H]-HMQC. The ^{15}N-^{1}H HSQC spectra were acquired with a ^{15}N spectral width of 5000 Hz (oxidized samples) and 3000 Hz (reduced samples), and reduced to 2400 Hz for all other experiments. The ^{13}C spectral widths were 6500 Hz for CBCA(CO)NNH, 6300 Hz for HNCACB, 6000 Hz for HNCA, HNCO, (HB)-CB(CGCD)HD and (HB)CB(CGCDCE)HE, 5000 Hz for ^{13}C-^{1}H HSQC, F_1 (C_α) of ct-HCACO and ^{1}H-TOCSY-relayed ct-[^{13}C,^{1}H]-HMQC, 3500 Hz for HCCH-TOCSY, 3000 Hz for ^{13}C-edited NOESY−HMQC and the F_2 (C′) of ct-HCACO. Quadrature detection for the indirectly detected dimensions in all experiments was achieved by States-TPPI method (*39*), with the exception of ^{15}N-^{1}H HSQC, in which TPPI was used. The number of complex points collected in the directly detected dimension was: 4096 for ^{15}N-^{1}H HSQC, ^{13}C-^{1}H HSQC, the 2D version of ct-HCACO with t_1 evolution on C′, the 2D version of HNCOCA with t_1 evolution on C_α and mq-HNCO; 2048 for (HB)CB(CGCD)-HD, (HB)CB(CGCD)HD, HNCA, and ct-HCACO; 1024 for all other experiments. The number of real points collected for the indirectly detected dimensions was 1024 in ^{15}N-^{1}H HSQC spectra, 1024 in ^{13}C-^{1}H HSQC and the 2D versions of ct-HCACO and HNCOCA; 700 in mq-HNCO; 45 in (HB)CB(CGCD)HD and (HB)CB(CGCDCE)HE; 68 (F_1) and 40 (F_2) in ^{1}H-TOCSY-relayed ct-[^{13}C,^{1}H]-HMQC; 70 (F_1) and 24 (F_2) in HNCO; 59 (F_1) and 20 (F_2) in HNCA; 60 (F_1) and 20 (F_2) in HNCACB; 43 (F_1) and 26 (F_2) in CBCA(CO)NNH; 80 (F_1) and 24 (F_2) in HBHA(CO)NNH; 128 (F_1) and 64 (F_2) in HCCH-TOCSY; 16 (F_1) and 55 (F_2) in ct-HCACO, 128 (F_1) and 49 (F_2) in ^{13}C-edited NOESY−HMQC and ^{15}N-edited NOESY−HMQC.

The number of transients acquired for each FID was 16 for all experiments on the free cyt b_5 except for the HCCH-TOCSY and CBCA(CO)NNH spectra, in which 8 and 32 transients were acquired, respectively, and 512 transients/FID for the (HB)CB(CGCD)HD and (HB)CB(CGCDCE)-HE spectra. For the cyt b_5−cyt *c* complex samples, 16 transients were acquired per FID for all experiments except for the following: 32 for ^{13}C-^{1}H HSQC, 64 for HNCA, and 96 for the 2D version of ct-HCACO. The mixing time used for all experiments, which included a NOESY transfer step, was 100 ms.

Spectra were processed using either our in-house program, Striker (*40*), or nmrPipe (*41*). Interactive spectral display and analyses were accomplished with our in-house program, Sparky (*42, 43*). Low-frequency filtering of the water signal in the directly detected dimension was used when appropriate. An apodization function of 70 or 80°-shifted sine-squared or a Gaussian window with 1−8 Hz of line broadening centering the maximum at the first 3−5% of the FID was applied to all dimensions before Fourier transformation. Linear prediction extension of the indirectly detected dimensions were used in HCCH-TOCSY and HBHA(CO)NNH.

For comparison between the free and complexed cyt b_5 in the ferrous state, the chemical shifts of the backbone amide ^{15}N and proton, $^{13}C_\alpha$ and H_α were used. For the free cyt b_5, backbone amide ^{15}N and proton resonances were obtained from ^{15}N HSQC, while the $^{13}C_\alpha$, as well as H_α resonances were from the F_2 and F_3 dimensions of HCCHTOCSY, respectively. The effects of low digital resolution and low signal-to-noise ratio on the accuracy of our chemical shifts were minimized by averaging the chemical shifts from different spectra. For the complex, the backbone amide ^{15}N resonances were averaged from the ^{15}N-HSQC and the mq-HNCO spectra; the $^{13}C_\alpha$ resonances were obtained from a 2D version of HNCOCA (t_1 evolution on $^{13}C_\alpha$), the H_α shifts were from the directly detected proton dimension (F_3) of HCCHTOCSY, and the backbone amide ^{1}H resonances were averaged from ^{15}N-HSQC, mq-HNCO, and HNCOCA. The spectral resolution in ^{15}N-HSQC, mq-HNCO, and HNCOCA (calculated without zero-filling) was 0.007 ppm (8000 Hz, 2048 real points), and 0.026 ppm (8000 Hz, 512 real points) in HCCH-TOCSY. The digital resolution was 0.05 ppm (3000 Hz, 1024 real points) in ^{15}N-^{1}H HSQC; 0.07 ppm (5000 Hz, 700 real points) in HNCOCA; 0.16 ppm (5000 Hz, 520 real points) in mq-HNCO (^{15}N); 0.072 ppm (5500 Hz, 128 real points) in F_1 (the indirectly detected proton dimension); and 0.365 ppm (3500 Hz, 64 real points) in the F_2 (carbon dimension) of HCCH-TOCSY.

The composite chemical shift change for the resonances of the backbone nuclei in each residue was calculated as the square root of the sum of the squares of the differences between the free and bound chemical shifts for each of the four backbone nuclei, with the differences in ^{15}N and ^{13}C divided by 4. The ^{15}N and ^{13}C differences were divided by 4 in order to put equal weight to all chemical shifts, since the chemical shift range of the amide protons is approximately one-fourth the chemical shift range for the amide ^{15}N shifts and the $^{13}C_\alpha$ shifts.

Measurement of the Diffusion Coefficients. Diffusion measurements were carried out with the sequence presented by Altieri and co-workers (*44*), using pulse field-gradient strengths of 2−45 G/cm applied for 7.5 ms each. Attenuation of the ^{1}H signal for each of the components in the sample of the complex of cyt b_5 with cyt *c* was determined by following well resolved peak heights for resonances that could clearly be identified as coming from either cyt b_5 or cyt *c*. The results were analyzed by a least-squares fit to eq 1:

$$A(\tau) = A(0)\exp[-(\gamma\delta\Gamma)^2\tau D_s] \qquad (1)$$

as a function and of gradient strength (Γ) using a time between gradients of 28 ms.

In eq 1, $A(\tau)$ is the signal intensity at time τ (s) between gradients, δ is the pulsed-field gradient duration (s), D_s is the diffusion coefficient (cm^2/s), and γ is the ^{1}H gyromagnetic ratio.

Molecular Dynamics Simulations. The "cleft complex" was formed by docking the heme-exposed face of cyt *c* into the hydrophobic cleft of cyt b_5 (*18*), observing proper steric packing at the complex interface. The "Salemme complex" was based on the original Salemme model utilizing electrostatic charge pairing of cyt *c* lysine residues (K13, K27, K72, and K79) and acidic residues in cyt b_5 (E48, E44, and D60) including the heme propionate) (*7*). The starting structure for the cleft complex simulation was a 1600 ps snapshot ("cleft opened" conformation) from the oxidized wild-type cyt b_5 bovine MD simulation (see ref *18* for a detailed description) and the NMR-derived solution structure of reduced horse heart cyt *c* [PDB accession number 2frc (*45*)]. To match the NMR studies, the iron atom was reduced in cyt b_5. The starting structures for the Salemme complex simulation were a 300 ps snapshot ("cleft closed" conformation) from the wild-type cyt b_5 bovine structure (*18*) and the same cyt *c* structure as used in the cleft complex simulation. Deamidation at Asn 17 occurs during the purification process, as described later in this paper. Therefore, an Asn17 to Asp modification was made to the cyt b_5 starting coordinates. In both simulations, cyt b_5 and cyt *c* were in the ferrous oxidation state, and ionization states corresponded to neutral pH.

Energy minimization and the MD simulations were performed using the program ENCAD (*46*). The potential energy function and associated protocols have been described (*47*). The heme parameters of Henry and co-workers (*48*) were used, except that the iron was reduced. The system consisted of the protein complex in a rectangular box of water molecules with walls at least 8 Å from any protein atom resulting in the addition of 6381 and 5854 water molecules, respectively, in the cleft complex and Salemme complex. The water density was set to the experimental value of 0.997 g/mL at 298 K by adjusting the volume of the box (*49*). The systems were subjected to a variety of preparatory steps as described elsewhere (*18*). Each simulation was carried out for 2 ns. An 8 Å force-shifted nonbonded cutoff was used, and the nonbonded list was updated every five steps. Structures were saved every 0.2 ps for analysis, resulting in 10 000 structures for each complex.

RESULTS

Resonance Assignment Strategy. Resonance assignments were first obtained for ferrous cyt b_5, and the results were used as the starting point for the backbone assignments of cyt b_5 in the ferrous cyt b_5−ferrous cyt *c* complex. For ferric cyt b_5, both free and complexed to ferric cyt *c*, the resonance assignments were initially transferred from diamagnetic ferrous cyt b_5, as described previously (*50*), and then expanded using the experimental results from the ferric system.

The scheme used in assigning the resonances in free ferrous cyt b_5, was to extend the ^{15}N-^{1}H backbone amide correlation, first to other backbone nuclei, H_α, C_α, and C′, and then to the side-chain nuclei. Initially, arbitrarily numbered backbone amide peaks in ^{15}N-^{1}H HSQC spectra were used, followed by a search for peaks with the same amide resonances in the HNCACB, CBCA(CO)NNH, HBHA(CO)NNH, and HNCO spectra. By use of these four 3D spectra in concert, almost all of the sequential backbone nuclei assignments were identified. A majority of the H_α and C_α resonances were assigned, as well. NOE spectra were used to close the remaining gaps in the sequential assignment process.

The assignment of side-chain nuclei was accomplished by extending the correlations from the C_α and C_β nuclei. The aliphatic ^{13}C-^{1}H assignments were based on the HCCH-TOCSY experiment. The assignment of side-chain carbonyl (as in Asn and Gln) and carboxyl carbons (as in Asp and Glu) were obtained from a 2D version of the HCACO experiments with t_1 evolution on the C′ resonance; this experiment correlated the H_β or H_γ protons with the side-chain carbonyl or carboxyl atom. A modified HCACO experiment, using a 13 ms spin lock pulse on the proton applied immediately before acquisition, was used to relay the H_β or H_γ proton magnetization to the H_α and H_β protons, respectively. This experiment helped to resolve some of the overlapped side-chain carbonyl or carboxyl carbon resonances of Asn, Asp, Glu, and Gln. The side-chain ^{15}N-^{1}H assignments, namely those of the amides of Asn and Gln; the ϵ-NH of Arg; the ϵ-amino group of Lys; the ϵ-NH of Trp, were based on ^{15}N-^{1}H HSQC, HBHA(CO)NNH, and HNCACB experiments. The aromatic residue side-chain assignments were accomplished by first correlating the known C_β resonances to their respective H_δ or H_ϵ resonances in the 2D (HB)CB(CGCD)HD and (HB)CB(CGCDCE)HE spectra. The assignments were then extended to other protonated carbons correlated to the H_δ or H_ϵ resonances in each of the aromatic rings with the combined use of the ^{13}C-^{1}H HSQC (optimized for aromatic carbons) and 3D ^{1}H-TOCSY-relayed ct-[^{13}C,^{1}H]-HMQC experiments. Results from a ^{13}C-edited NOESY−HMQC experiment optimized for aromatic carbons were used to confirm some of the aromatic side-chain assignments.

Assignment of Backbone Nuclei in Free Ferrous Cyt b$_5$. All of the 79 protonated backbone amide resonances expected for the 82 residue recombinant ^{15}N and ^{13}C-uniformly labeled cyt b_5 were observed in the ^{15}N-^{1}H HSQC spectrum. With the exception of overlap between the resonances of E56 with F58, in both the ^{15}N and ^{1}H dimensions, all amide resonances were resolved in this spectrum. However, 27 additional amide resonances at smaller peak intensities were also observed. The origin of these extra peaks will be discussed later. Complete backbone assignments for the observable ^{15}N, ^{13}C, and ^{1}H resonances of 78 of the 82 residues were obtained from scalar connectivities while the remaining 4, S20 to T21, H26 to Y27, H39 to P40, and H80 to P81, were determined by the connectivities observed in ^{13}C-edited and ^{15}N-edited NOESY spectra.

The current assignments on the ^{13}C-^{15}N labeled ferrous cyt b_5 are in good agreement with the previous proton assignments with the unlabeled protein (*51*). Of the 78 amide proton resonances assigned in both of our studies, 76 differed by 0.2 ppm or less. The two exceptions were the amide protons of S18 and G41, which differed by 0.84 and 5.15 ppm, respectively. The previous assignments of S18 and G41 were complicated because the “fingerprint” amide proton−α proton correlation peak of S18 was not observed, and the G41 amide was assigned to be coincident with that of G42. These ambiguities have now been resolved based on scalar connectivities to their respective preceding and succeeding residues, through the use of heteronuclear correlations.

Assignment of the Resonances of the Side-Chain Nuclei in Free Ferrous Cyt b$_5$. (a) Aliphatic side chains. The assignment of the aliphatic ^{13}C and ^{1}H side-chain resonances in free ferrous cyt b_5 was straightforward, and almost all were assigned except for the following: C_δ and H_δ of K5; $C_{\delta 1}$, H_δ, $C_{\gamma 2}$, and H_γ of I12; C_ϵ and H_ϵ of K14; C_γ of Q59; C_γ of R68; C_ϵ and H_ϵ of K72. The assignment of Lys and Arg side chains was difficult due to severe overlap. The degeneracy between H_δ and H_γ of I12 could not be resolved.

(b) Aromatic Side Chains. The correlation peak observed between the H_δ and C_β resonances of W22 in the (HB)CB(CGCD)HD spectrum established the linkage from the main chain to its aromatic side chain. The resonances in the benzene ring of W22 were assigned to a set of five relay peaks, identified in the ^{1}H-TOCSY-relayed ct-[^{13}C,^{1}H]-HMQC spectrum. In addition, minor peaks were observed for W22, which may be the result of a 180° rotation of the indole ring. Relay peaks between the H_δ of W22 and the remaining aromatic protons of W22 were not observed. However, an intraresidue NOE peak observed between the H_β and $H_{\zeta 2}$ protons of W22 in the ^{13}C-edited NOESY spectrum optimized for aromatic carbons provided the confirmation that these resonances belong to W22. The indole NH resonance was observed only in the ^{15}N-^{1}H HSQC spectrum; this assignment was based on a comparison with previous results (*51*).

The H_δ resonances of the five histidines (H15, H26, H39, H63, and H80) were identified in the (HB)CB(CGCD)HD spectrum from correlation peaks to the their respective C_β resonances. The assignment of the C_ϵ and H_ϵ resonances of the nonaxial histidines (H15, H26, and H80) observed in the gradient-enhanced ^{13}C-^{1}H HSQC spectrum optimized for aromatic carbons were based on previous results with ferric cyt b_5 from reference (*25*); these residues are away from the paramagnetic site, and their chemical shifts are expected to be the same in both the oxidized and reduced states. A cross-peak with 131.84 ppm ^{13}C shift and 1.31 ppm ^{1}H shift and another with ^{13}C and ^{1}H shifts at 132.21 and 0.82 ppm were observed in the gradient-enhanced ^{13}C-^{1}H spectrum optimized for aromatic carbons, but were not assigned; however, the large upfield shifts of the ring protons, for these cross-peaks to carbon shifts in the aromatic range, are consistent with the large heme-induced shift effect expected for the axial histidines, and they correspond, most likely, to the C_ϵ-H_ϵ of H39 and H63. No NOESY peaks were observed from these resonances, so they are not assigned.

The tyrosine (Y6, Y7, Y27, and Y30) aromatic side chains were assigned. The aromatic side-chain assignments for the phenylalanines (F35, F58, and F74) are less complete: F35 has been completely assigned, the F74 side chain has been assigned except for the C_δ resonance, and F58 has been assigned tentatively, based on comparison with results from (*51*). The difficulty in assigning the F58 side chain was due to the lack of a C_β−H_δ correlation peak in the (HB)CB(CGCD)HD spectrum. Several ^{13}C-^{1}H aromatic resonances (129.4−7.42, 129.4−7.34, 112.29−7.50, and 127.92−7.38) were not assigned due to the lack of cross-peaks to resonances that could be linked to the backbone atoms.

Two H_ϵ resonances were observed for the axial histidines, H39 and H63, with their chemical shifts near 1 ppm, which is upfield of the corresponding random-coil shifts by about 7 ppm. This is consistent with a large ring current shift due to their location immediately above and below the heme. It was not possible, however, to conclude which of these two histidines gave rise to which resonance. Recently, Guiles and co-workers (*52*) reported a similar large ring current shift in rat cyt b_5, with its G41 amide proton at 1.1 ppm. A complete list of resonance assignments for ferrous cyt b_5 is given in Table 1 of Supporting Information.

Observation and Identification of Resonances Due to Heterogeneity of the Free Ferrous Cyt b$_5$. As mentioned earlier, 27 extra cross-peaks, with lower intensity than the other cross-peaks, were observed in the ^{15}N-^{1}H HSQC spectrum. Sequential assignments could be made for most of these cross-peaks as they correlated to previous or subsequent residues of the major component.

Previous NMR experiments have established that bovine cyt b_5 exists in two forms which occur in a 1:9 ratio. These two forms arise from a 180° rotation of the heme about its α,γ-meso axis (*53*). In our spectra, several of the extra cross-peaks had their intensities in approximately a 1:8 ratio to the corresponding major peaks, in agreement with this heme reorientation hypothesis. A "double-half-filtered" NOESY experiment (*54*), observing only the unlabeled resonances in free ferrous cyt b_5, showed a major and a minor set of heme resonances at a ratio of 8.5:1. This is because cyt b_5 is expressed as the apo protein and exogenous unlabeled heme was added to reconstitute the holoprotein. On the basis of the intensities in the ^{15}N-^{1}H HSQC spectrum, the major-to-minor ratios of L32, H39, G42, V61, L36, K72, and L70 ranged from 6.1 (G41) to 12.6 (S64). All of these residues are located near the heme. The wide range of these ratios could be due to the proximity of these peaks to the major peaks or to underlying unresolved minor peaks.

Many of the extra cross-peaks, however, were much more intense with a ratio around 1:2 to the major component. Examination of all chemical shift differences between the major and minor components that were not due to heme reorientation revealed the largest such shift difference of 1.9 ppm between the β-carbon shifts of the minor and major forms for N17. This suggests that deamidation could be the source of these extra resonances. To determine whether this residue was an asparagine or an aspartate, we obtained 2D versions of the ct-HCACO experiment with and without ^{15}N decoupling. The characteristic 14 Hz coupling between the C′ and N nuclei in the amide bond of asparagine and glutamine residues was observed in the experiment without ^{15}N decoupling. This coupling was not observed for residue 17 in the major species, identifying the major component as the N17D variant. The 14 Hz coupling was observed for the minor component for residue 17, identifying it as N17, as expected for wild-type cyt b_5. This splitting disappeared with ^{15}N decoupling. Several residues in the vicinity of residue 17 (Y6, T8, E11, I12, K14, H15, T21, and W22) were affected by the deamidation, as they had an average of about 1−1.6 for the ratio of the minor to major species. The ratios for N16 and S20 were 1:2 and 1:3, respectively.

The relative amount of N17D to the wild-type protein was assessed by comparing the ^{15}N-^{1}H correlation peak height ratios of N17 and D17. The extent of deamidation increases with the amount of time in the oxidized form. While there was no change in the reduced sample of cyt b_5 over a period of a few years, the N17D to wild-type protein ratio in the first ferrous cyt b_5 sample was about 1.5:1. In the second ferrous cyt b_5 and other oxidized cyt b_5 samples, the ratios were 2 to 1 and 3.5 to 1, respectively. As described in Materials and Methods, the second ferrous cyt b_5 NMR sample, as well as oxidized cyt b_5 NMR samples were prepared with material from the first 9 mM ferrous cyt b_5 sample. The cyt b_5 in the ferrous cyt b_5−cyt *c* complex sample was prepared from material that had been stored at −70 °C in the oxidized form for more than a year and appears to be fully deamidated. All of the cyt b_5 protein studied was derived from a single preparation of cyt b_5.

To compare the chemical shifts of cyt b_5 in the free and bound states, only the deamidated species is considered, since the wild-type protein is not present in the ferrous cyt b_5−ferrous cyt *c* sample and only at a very small proportion in the oxidized system. The assumption that the deamidated and the wild-type proteins are similar is made, and it is based on the following observations. A comparison of the secondary structure of N17D, as obtained from analysis of the NOESY spectra, with that of the reduced crystal indicates a good agreement between the two. In addition, the equilibrium heme isomer ratio in ferrous cyt b_5, measured directly from the heme resonances in ferrous cyt b_5, was 8.5:1, which is not significantly different from that of the reported ratio of about 9:1 for the wild-type protein. These data suggest that the overall structure and the equilibrium heme-binding properties of N17D are similar to that of the wild-type protein.

Resonance Assignments of Backbone and Side-Chain Nuclei in the Ferrous Cyt b_5*−Ferrous Cyt c Complex.* Backbone and side-chain assignments in ferrous cyt b_5 in complex with ferrous cyt *c* (1 mM:1.2 mM, at pH ∼6.5) were based on our assignments of free ferrous cyt b_5. The backbone amide assignments for the complex were first obtained from overlaid ^{15}N-^{1}H HSQC and 2D-HNCOCA spectra from free and complexed cyt b_5 and then confirmed in the HNCA experiment on the bound cyt b_5. A mq-HNCO spectrum was used to help resolve overlap in the ^{15}N and ^{1}H amide dimensions. The side-chain assignments were obtained from the HCCH-TOCSY and ^{13}C-^{1}H HSQC spectra optimized for aromatic carbons. As expected from a decrease in transverse relaxation time of cyt b_5 when complexed with cyt *c*, many cyt b_5 peaks, especially those of the side chains, have broadened. This resulted in peak overlaps and disappearance of peaks. As a result, the resonance assignments of cyt b_5 in the ferrous complex are less complete than those of the free ferrous cyt b_5. Nevertheless, backbone assignments were made for all residues in the ferrous cyt b_5 complex with cyt *c*, except for the N-terminal amine at A3 and the amide of S18. It should be noted that cyt b_5 is almost completely deamidated at residue 17 in the ferrous cyt b_5−cyt *c* complex, and residue 17 is referred to as "D17".

The ^{15}N-^{1}H cyt b_5 amide peaks of T33, E48, D53, T55, E56, N57, F58, E59, and D83 in the ferrous complex could not be resolved from overlapping peaks in the HSQC spectrum. However, with the exception of D53 and T55, all of these peaks were resolved in the mq-HNCO spectrum. In a 2D-HN(CO)CA experiment (with t_1 evolution on C_α), the correlation peaks between the amide proton of D53 and T55 and the C_α of their respective preceding residues were identified. The amide resonance of S18 was not observed, possibly due to an increase in line width from exchange between different forms of the complex. Line-broadening effects rendered the assignment of the following peaks very difficult: C_γ of T8; $C_{\delta1}$,$C_{\delta2}$,C_γ of L9;$C_{\gamma1}$, $C_{\gamma2}$ of I12; C_β, C_γ, C_δ and C_ϵ, of K19; C_β of K34; C_β, C_γ, C_δ and C_ϵ, of R47; C_β of F58; C_α of S64; C_α, C_γ and C_δ of R68; C_α and C_γ of E69; C_δ of K72. These peaks could not be resolved from other peaks in the HCCH-TOCSY spectrum. In addition, the HCCH-TOCSY peaks of the following residues in cyt b_5 became so weak or disappeared upon complexation with cyt *c* that they were not assigned: C_β of Y7; C_α and C_β of H15; C_β of N16; C_α and C_β of S20; C_β and C_γ of T21; C_β of L25; K28; C_β of Y30; C_β of D31; P40; C_β and C_γ of Q49; C_β of D53; C_β of N57; E59; C_β of H63; S71; C_γ of K72; C_β of F74; C_β of L79; C_β of D83; R84. Moreover, with the exception of D60, it was not possible to detect the side-chain carbonyl or carboxyl resonances of other Asn, Gln, Asp, and Glu residues in cyt b_5 in the ferrous complex 2D−

H(CA)CO spectrum, which correlates protons to the adjacent carbonyl or carboxyl carbon. The inability to observe these peaks is presumably due to an increase in line widths via the chemical shift anisotropy mechanism for the carbonyl or carboxyl carbons. The efficiency of this relaxation pathway is particularly enhanced as the correlation time of the molecule increases upon complexation. A general line-broadening effect was also observed in the ^{13}C-^{1}H HSQC spectrum optimized for the aromatic carbons of ferrous cyt b_5. The broadening was so severe that the following peaks could not be assigned: the $C_{\eta 2}-H_{\eta 2}$ peak of W22; C_δ and C_ϵ peaks of Y30; C_δ and C_ϵ peaks of F35; C_δ peaks of H63, F58, and F74; the C_ϵ of F35. The complete listing of resonance assignments of ferrous cyt b_5 in complex with cyt *c* is given in Table 2 of the Supporting Information.

Assignment of the Backbone Resonances of Ferric Cyt b_5. The resonance assignments of ferric cyt b_5 were obtained for the backbone nuclei (N, H^N, C_α) and the histidine side chains only. The assignment of the backbone nuclei of paramagnetic ferric cyt b_5 was accomplished by transferring all possible assignments from the diamagnetic system (*50*). These starting points were then used to complete the sequential assignments with the use of the HNCA spectrum. Side-chain assignments for the histidines were based on previous experiments from this laboratory (*25*). The rationale for the assignment transfer technique from the diamagnetic ferrous cyt b_5 to the paramagnetic ferric cyt b_5 is based on a variety of observations: assuming that the structure is the same in the oxidized and reduced states (*55*), the pseudocontact shifts experienced by the protons and the heteronuclei, ^{13}C and ^{15}N, are of the same absolute magnitude for a given location in the molecule. However, the pseudocontact shifts for the ^{13}C and ^{15}N nuclei are small ($\cong$0.1 ppm) compared to the usual ^{13}C and ^{15}N nuclei chemical shifts of several parts per million caused by differences in the local magnetic environment. Such apparent insensitivity of the heteronuclei chemical shifts to oxidation states can be exploited for resonance assignment purposes: analogous resonances in the two oxidation states might be related by a small shift in the heteronuclear dimensions, accompanied by possibly a larger shift, generally in the same direction, in the proton dimension.

In the current work, an initial set of backbone assignments for ferric cyt b_5 was obtained by studying the magnitude and directions of relative shifts in both the proton and heteronuclear dimensions in the overlaid sets of ^{15}N-^{1}H HSQC and 2D-H(NCO)CA spectra in the diamagnetic and paramagnetic states. Using the HNCA spectrum and the above initial set of backbone assignments, we have obtained backbone assignments for all ferric cyt b_5 residues, except for A3 and P40. The terminal amine of A3 was not observed, as expected due to rapid hydrogen exchange with the solvent. The amide resonances of S20, G41, and L70 were not observed, but their respective α-carbons were assigned. The C_α resonances of K19, H39, E69, and H80 were not observed, but their amide resonances were assigned.

A comparison of our ferric cyt b_5 backbone assignments with those reported by Whitford and co-workers (*6*) on a 103 residue uniformly ^{15}N-labeled bovine ferric cyt b_5 indicates general agreement in view of the differences in sample conditions between the two studies. However, there are some assignment differences that should be noted since some of the backbone amide chemical shifts assigned by Whitford and co-workers differed from ours in the ^{15}N dimension by more than 4 ppm and in the ^{1}H dimension by more than 1 ppm. In the following enumeration of the discrepancies between some of our assignments and those of Whitford, the assignments of Whitford are given in square brackets followed by the differences between their chemical shift and ours: I12 ([114.9, 7.96], −6.7, −0.44); Q13 ([114.4, 6.94], −1.1, −1.27); N16 ([122.4, 8.17], 5.1, 0.85); S18 ([125.2, 7.89], 11.9, −0.29); K34 ([120.0, 7.41], 2.9, −1.5); H39 ([114.9, 8.88], −5.8, 0.27); E69 ([119.6, 7.01], −3.8, −2).

The differences at N16 and S18 might be due to deamidation in our cyt b_5 at position 17. However, if the backbone ^{15}N-^{1}H assignment of N17 by Whitford and co-workers (*6*) at 118.7 and 7.74 ppm were transposed with their N16 assignments, then the shift discrepancies of the backbone amide at residues 16 and 17 between the two studies would be (1.4, 0) and (1.4, 0.42), respectively, which are within the range attributable to differences in sample conditions. All resonance assignments of ferric cyt b_5 are listed in Table 3 of the Supporting Information.

Assignment of the backbone resonances of ferric cyt b_5 bound to ferric cyt *c*. Resonance assignments in ferric cyt b_5−ferric cyt *c* were transferred directly from the free ferric cyt b_5. The sequential assignments were confirmed with results from the HNCA experiment. The chemical shift assignments of ferric cyt b_5 complexed to ferric cyt b_5 are listed in Table 4 of the Supporting Information.

Determination of the pH Dependence of the Chemical Shifts in Free Ferric Cyt b_5 and in Complex with Ferric Cyt c. The chemical shift changes observed between the free and bound forms could originate not only from complex-induced mechanisms, including pseudocontact shifts, but also from a small variation in the pH of the two samples, especially if the pH of both samples are at or near the pK_a of the titratable group. To control for these possible pK_a-induced chemical shift changes in the free and bound ferrous cyt b_5, the chemical shifts of the ionizable residues and their neighboring amino acids in ferric free and bound cyt b_5 were measured as a function of pH between pH 6 and 9 in the ^{15}N-^{1}H HSQC spectra and the ^{13}C-^{1}H HSQC spectra optimized for aromatic residues. We assume that the pK_as are the same in both oxidation states. The pH titrations were performed on ferric proteins because the pH of the ferrous samples could not be controlled. The residues whose side chains titrate near pH 6.5, as well as their neighbors, could then be excluded from subsequent analysis on complex-induced chemical shift changes, since the contributions from these two mechanisms could not be quantitated.

Only four residues in bovine cyt b_5 (H15, H26, H80, are A3) are expected to titrate between pH 6.5 and 8.5. The pK_a values of the nonaxial histidines in bovine ferric cyt b_5 had been previously determined to be 8.47, 6.92, and <5.5, respectively (*25*). Extremely efficient relaxation by the paramagnetic iron rendered the $^{13}C_\epsilon$-^{1}H correlation peaks of the axial histidines unobservable in the oxidized cyt b_5 samples. Our results indicate that the titration profiles of the nonaxial histidines, determined from the imidazole C_ϵ1H resonances (Figure 2), are similar in the free and complexed cyt b_5. In addition, the experimentally determined pK_as agree with the previous results (*25*). The amide resonances of all

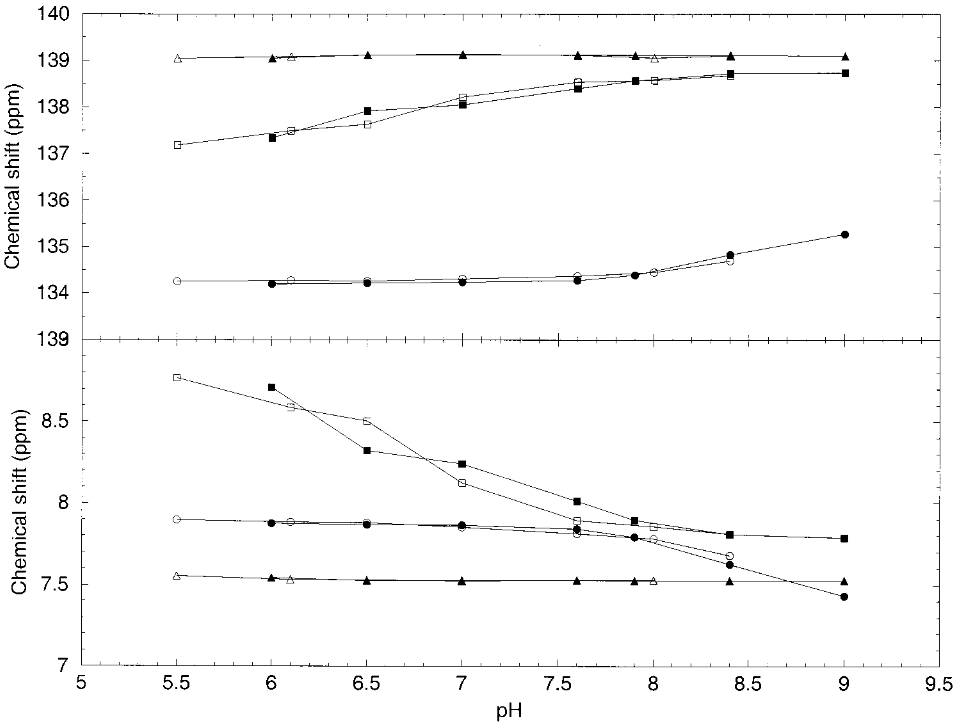

FIGURE 2: pH titration of the histidines (H15, H26, and H80) of cytochrome b_5 in ferric cytochrome b_5 (closed circle, square and triangle, respectively) and ferric cytochrome b_5−ferric cytochrome *c* (opened circle, square, and triangle, respectively). The imidazole C_ϵ and H_ϵ chemical shift changes relative to values observed at the lowest pH are plotted as functions of pH, respectively, in the upper and lower panels.

residues undergo negligible perturbations near pH 6.5 in both the free and complexed ferric cyt b_5, except for H26, since its pK_a is 6.92 (*25*). On the basis of the above findings, H26 is excluded from consideration in complex-induced chemical shift changes.

Analysis of the Chemical Shift Changes Which Occur upon Binding of Ferrous Cyt c to Ferrous Cyt b_5. To determine which cyt b_5 amino acids were involved in complex formation to cyt *c*, the chemical shifts of backbone amide ^{15}N and proton and $^{13}C_\alpha$ and H_α of the ferrous cyt b_5 in complex with cyt *c* were compared with those of ferrous cyt b_5. The concentrations of cyt b_5 and cyt *c* were 1 and 1.2 mM, respectively. Small chemical shift changes (less than 0.10 ppm for backbone proton, less than 1.03 ppm for backbone nitrogen, less than 1.15 ppm for backbone ^{13} C_α and less than 0.16 ppm for the H_α), were observed for a number of residues in cyt b_5. To combine the results of all the backbone resonances, a composite chemical shift difference was calculated as the weighed mean of the differences between the free and bound chemical shifts for each of the four backbone nuclei, as described in the Experimental Section. The composite differences between ferrous cyt b_5 free and bound to ferrous cyt *c*, as well as the differences between ferric cyt b_5 free and bound to ferric cyt *c*, are shown in Figure 3. Composite differences greater than the geometric mean of the values for all residues in cyt b_5 in the reduced species were considered to be of significant magnitude to indicate the effects of cyt *c* binding. The residues that fell into this category are indicated on the structures shown in Figure 4.

Although the side-chain resonances of cyt b_5 were assigned in the free and bound ferrous state, they were not included in the above chemical shift comparisons for the following reasons. The chemical shift information of many cyt b_5 side-chain peaks in the complex was obliterated by the broadening of the peak due to the increase in rotational correlation time of cyt b_5 in the protein complex. To assign a single chemical shift change value to each residue, a composite chemical shift change upon binding must be generated. Including side-chain resonances would magnify the changes in the residues containing long side chains. Using only the backbone atoms ensures that there is no bias in the resulting composite calculated. The cyt b_5 residues that showed composite chemical shift changes of greater than 0.06 ppm (the geometric mean of all the composite shift differences) are divided into two classes. The first class contained residues whose composite changes were greater than or equal to 0.06 but less than 0.117 ppm (this value corresponds to the geometric mean of all the composite shift differences plus one standard deviation), while the second class of residues exhibited a change of greater than or equal to 0.117 ppm. The residues that showed changes of more than 0.117 were Y6 of helix α1, H15, D17, S18, K19, and S20 in the loop region connecting helix α1 and *β* strand *β*4; W22 in *β*4; H26 in the loop region that connects strands *β*4 and *β*3; E37 in α2; G51 in *β*5, T55 at the end of strand *β*5 (see Figures 3 and 4).

Most of the residues that showed smaller composite shift changes, between 0.06 and 0.117 ppm, upon complex formation, are located either in the four helices that form the heme-binding pocket (T33, K34, F35, L36, E38 in α2, V45 and R47 in α3, E59 in α4, L70 in α5), or in the *β*-sheet that forms the bottom of the pocket (T21 and L23 in *β*4; G50 in *β*5). In addition, G62, the axial ligand H63 and the loop linking α3 and *β*5 (E48, Q49, and A50), as well as A54 at the end of strand b_5, are affected. D82 also showed significant changes. A chemical shift perturbation was observed for H26. However, the pK_a of H26 has been

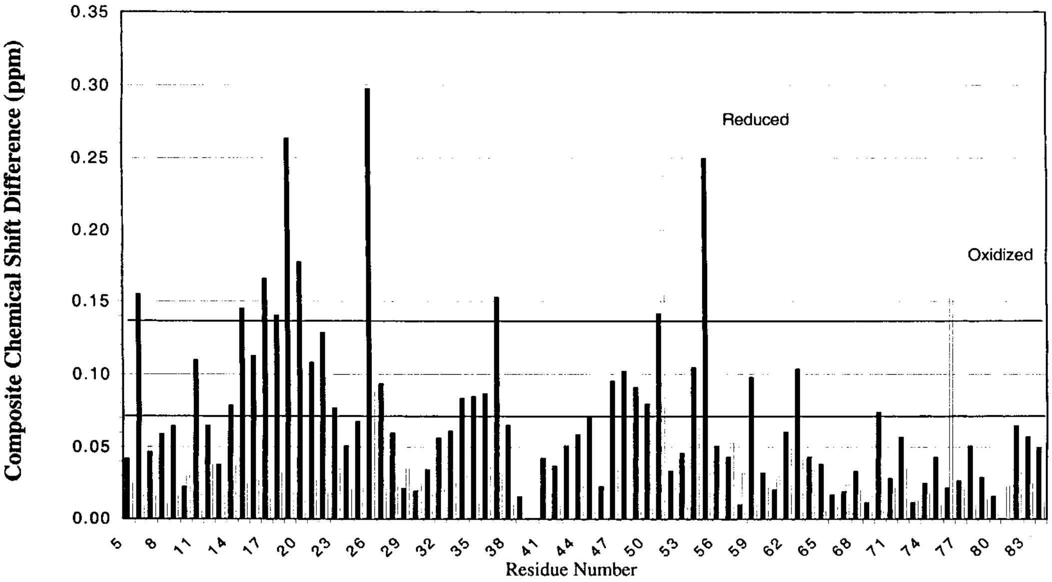

FIGURE 3: Composite chemical shift changes of backbone atoms in reduced and oxidized cyt b_5 upon binding to cyt *c*. The changes observed for the reduced and oxidized cyt b_5 upon complex formation to cyt *c* are shown in filled and open bars, respectively. The composite shift changes are calculated as indicated in the Experimental Section. Residues with composite chemical shift changes greater than 0.06 ppm (the mean of all composite chemical shift difference values in the reduced state) are considered significantly affected upon complex formation. Many residues were observed with composite shift changes greater than 0.117 ppm (i.e., greater than the mean composite difference plus one standard deviation from the mean).

determined to be approximately 6.5−7.0 in the free or bound oxidized form, near the pH at which the NMR spectra were obtained. Therefore, slight changes in experimental conditions could affect the chemical shifts for H26, so its shift changes were excluded from our analysis. The only other residue whose side-chain titrates in the range of 6−8 is H15; its pK_a, in both free and complex forms, has been determined to be greater than 7.5. The amine group at the N-terminus A3 has been predicted to titrate in the range of pH 6−8, but this does not affect our study since this amine group was not observed.

Measurement of Chemical Shift Changes That Occur on Ferric Cyt b_5 upon Binding Ferric Cyt c. The chemical shift differences between free and complexed ferric cyt b_5 are much smaller than those observed for the ferrous state. The largest complex-induced chemical shift change was 0.24 ppm observed for G51, while smaller differences (greater than 0.06 ppm) were observed for H26, A54, and I76. The composite chemical shift change of 0.09 ppm observed at H26 was not considered since the pH of the sample is in the titration range of its imidazole side chain. It should be noted that the following resonances were not observed in the ferric complex, presumably due to broadening of the peaks upon complex formation with cyt c: $^{13}C_\alpha$ of K19; ^{15}N amide of S20; $^{13}C_\alpha$ of L32; $^{13}C_\alpha$ of T33; $^{13}C_\alpha$ of H39; $^{13}C_\alpha$ of P40; G41; $^{13}C_\alpha$ of F58; $^{13}C_\alpha$ of G62; $^{13}C_\alpha$ of H63; $^{13}C_\alpha$ of I75.

Determination of the Diffusion Coefficients of the Free and Bound Forms of Ferrous Cyt b_5. The stoichiometry of the cyt b_5-cyt *c* complex was estimated by measuring the diffusion of free and bound cyt b_5 using pulsed field gradients as described in previous experiments (*54*). The results were the following: for free ferrous cyt b_5, the diffusion coefficient was $(1.13 \pm 0.01) \times 10^{-6}$ cm^2/s; for ferrous cyt b_5 in our 1:1.2 mixture with ferrous cyt *c*, it was $(0.72 \pm 0.01) \times 10^{-6}$ cm^2/s, and for complexed ferrous cyt *c* it was $(0.82 \pm 0.01) \times 10^{-6}$ cm^2/s. Assuming the molecular weight of 9966 for cyt b_5 (determined by mass spectrometry), we can estimate the apparent molecular weight for cyt b_5 in the complex with cyt *c* as approximately 23 880. The sum of the molecular weights of cyt b_5 and cyt *c* is 22 666, which is very close to the estimated molecular weight of the complex, and therefore these two molecules are bound in approximately a 1:1 stoichiometry. Complexed cyt *c* has a somewhat faster diffusion coefficient than complexed cyt b_5. This is presumably due to the existence of free cyt *c*, which was added in 20% excess, in fast equilibrium with cyt *c* bound to cyt b_5. It should be noted that this diffusion measurement is a bulk measurement and only reflects the equilibrium dissociation constant, K_d. This measurement is not sensitive to the exchange rates of the complex.

Molecular Dynamics Simulations of Two Cyt b_5−Cyt c Complexes. The amino acids in ferrous cyt b_5 whose backbones undergo chemical shift changes of 0.06 ppm or greater upon complexation with cyt *c* are illustrated in Figure 4. There are two main areas on ferrous cyt b_5 that exhibit significant changes. The first is the negatively charged anionic surface surrounding the heme. This is where Salemme (*7*) predicted the cationic surface of cyt *c* would bind (see the center panel at the top and the Salemme binding surface in Figure 4). The second area exhibiting noteworthy chemical shift changes on the left side of the molecule is depicted at the top of Figure 4, which is a region that exhibited heightened mobility in a molecular dynamics simulation of cyt b_5 (*18*). The mobility in this area leads to formation of a cleft that allows access to the hydrophobic core and the heme. In addition, it has been demonstrated that a genetically engineered salt bridge and disulfide bond designed to limit the motion of the loop was effective in dampening the cleft fluctuations (*56*, *57*). To explore the possibility that cyt *c* might bind to cyt b_5 in this transient cleft area, molecular dynamics simulations of cyt *c* bound to cyt b_5 at both the Salemme and cleft binding surfaces were performed (Figures 4 and 5). The starting structures for each simulation were either the cleft closed (for the Salemme

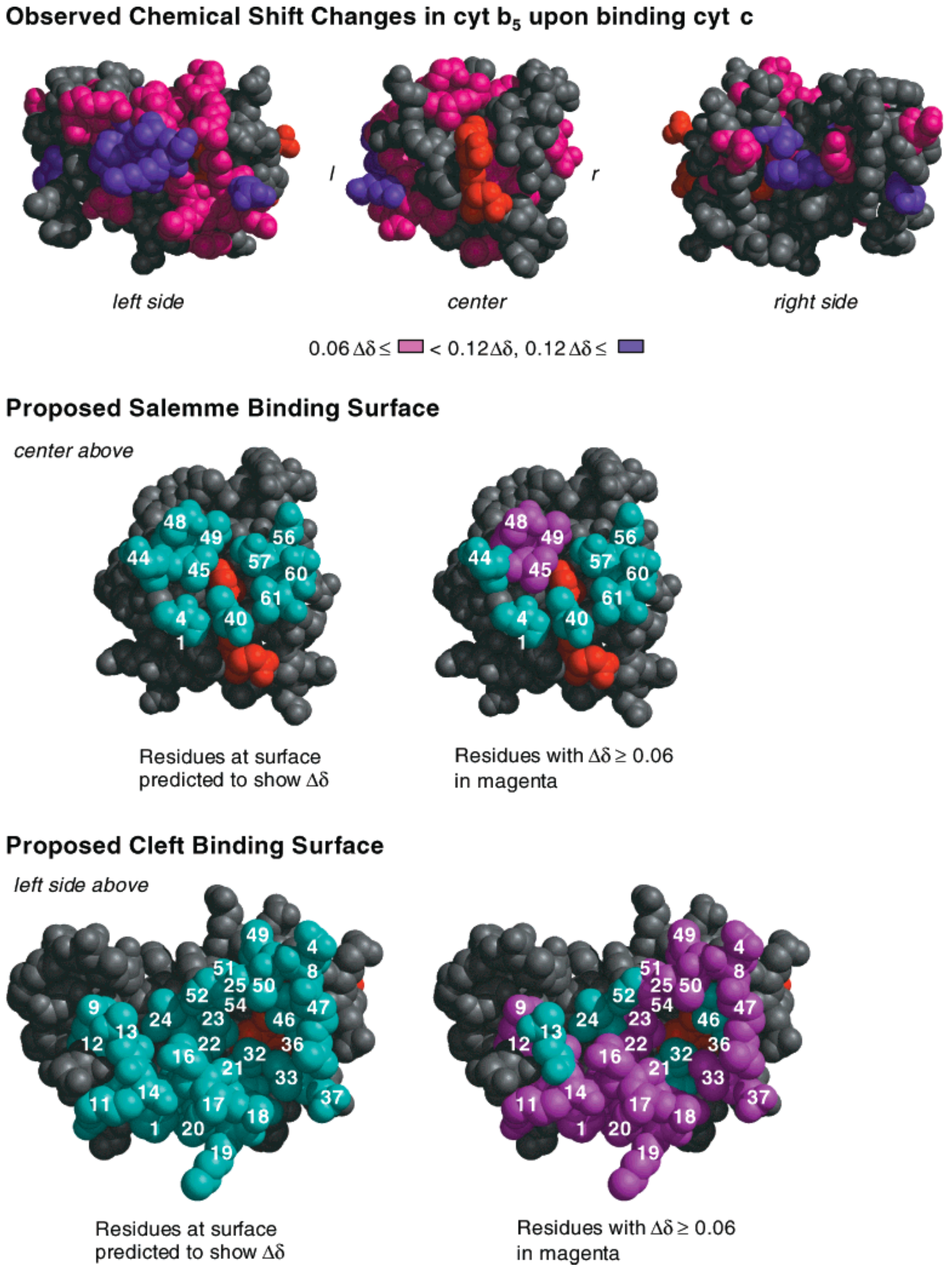

FIGURE 4: Observed chemical shift changes of cyt b_5 upon complex formation with cyt *c* and their distribution on the surface of the protein. The observed chemical shift changes from Figure 3 are displayed on the surface of cyt b_5 (note that some residues are below the surface). Moderate changes (0.06−0.12 ppm) are colored pink and larger changes (>0.12 ppm) are in purple. In every case the heme is red. The bulk of the residues affected fall near the heme on the Salemme binding surface (center structure) or the left side, which is the proposed cleft region. Residues displayed on the right side are near His 26 (shown in purple). The residues predicted to comprise the binding surface in the Salemme model are shown in cyan in the center strip. The residues that actually display shifts upon complex formation are colored magenta in the structure to the right. Finally, the predicted cleft surface is shown at the bottom in cyan and the residues actually undergoing a change are shown in the neighboring structure in magenta.

model) or cleft opened (for the cleft complex) conformations of cyt b_5 and the NMR-derived solution structure of cyt *c* (*45*). The starting structures for the complexes were hand docked, and packing at the interface was optimized. To test the stability of the complexes as a function of time and in the presence of water, MD simulations were performed for 2 ns. Equilibration of the simulations was judged by analysis of different structural characteristics (radius of gyration, change in accessible surface area, C_α root-mean-square deviation, etc.) and was deemed to have occurred when a plateau in the values was reached, which occurred between 0.5 and 1.0 ns (Figure 6).

The Salemme complex in Figure 5 was docked with optimal distances between four salt bridges, K13, K27, K72, and K79, in cyt *c* and E48, E44, D60, and the heme propionates in cyt b_5, as described previously (*7*). The salt bridges were maintained throughout the simulation and the hydrophobic packing at the interface became more favorable over time, as evidenced by a decrease in the interatomic Fe distances from 17 to 15 Å (SD ≈ 0.5 Å), and an increase in

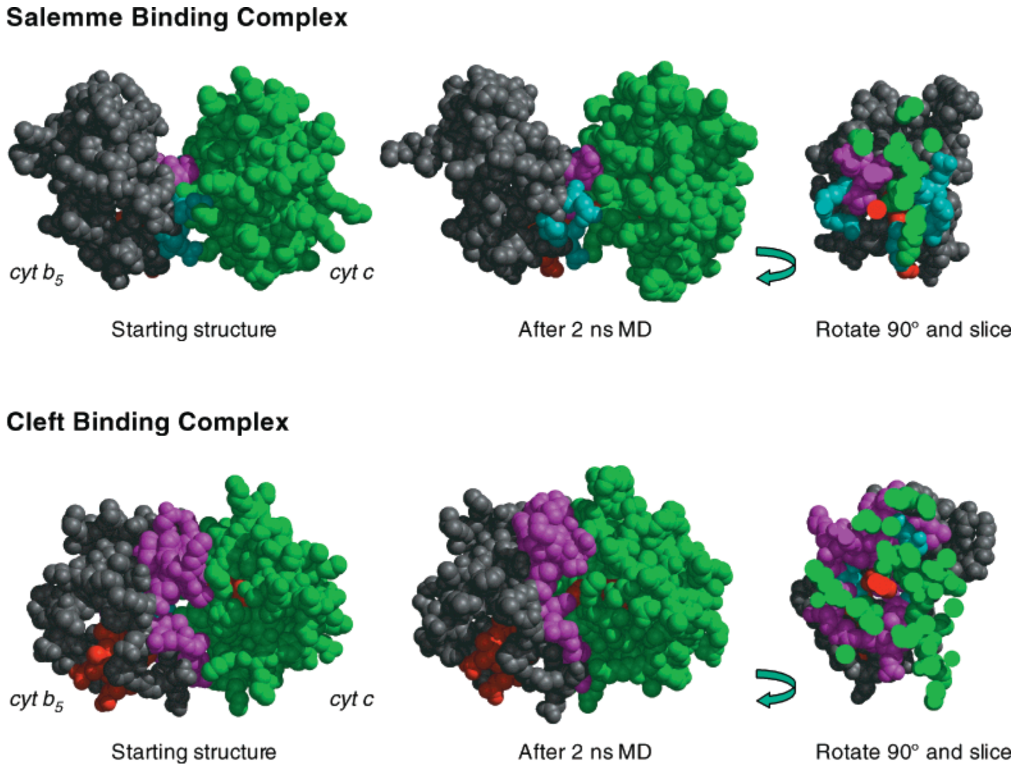

FIGURE 5: Simulated cyt b_5−cyt c complexes. The starting and final, 2 ns structures are displayed. Cyt c is shown in green. The residues predicted and observed to change upon complex formation are displayed in magenta and those that are predicted to change but do not are colored cyan (coloring as per Figure 4).

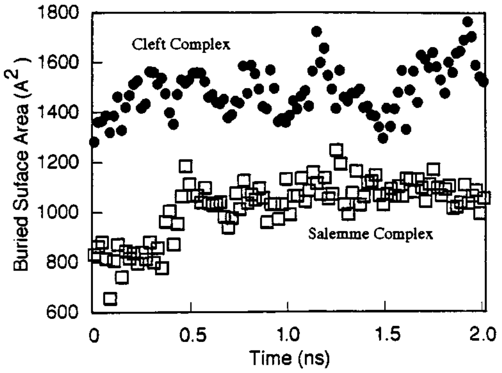

FIGURE 6: Buried surface area at the protein complex interface as a function of simulation time. The "Salemme complex" is shown in open squares and the "Cleft complex" is represented by filled circles.

the buried surface area at the complex interface (Figure 6). In the complex, the average C_α root-mean-squared (RMS) deviation from the starting structure was ∼2 Å. The highest deviations were due to residues 15−18, 40−43, and 49−53.

In the cleft complex, the exposed heme edge of cyt c was manually docked into the opened cleft of cyt b_5 (Figure 5). No salt bridges were present in the starting complex. By 100 ps, however, two intermolecular salt bridges (E10−K27 and E43−K72 in cyt b_5 and cyt c, respectively) had formed, each flanking one side of the binding surface. These residues were also involved in additional ionic interactions: K14 (cyt b_5)−E10 (cyt b_5); K27 (cyt c)−E21 (cyt c), and R47 (cyt b_5)−E43 (cyt b_5)−K72 (cyt c). As the simulation progressed, the packing at the interface became more favorable (Figures 5 and 6), and the interatomic Fe distance decreased from 25 to 21 Å (SD ≈ 1.0 Å). While the iron distances are longer in this complex, the path between the iron centers is hydrophobic and lined with aromatic residues (Figure 7). The buried surface area at the interface in the cleft complex was considerably larger than in the Salemme complex 1500 Å^2 versus 1000 Å^2, respectively (Figure 6). The difference is evident when comparing the binding surfaces of the two complexes (Figure 5). The average C_α RMS deviation of cyt b_5 from the starting structure was ∼1.7 Å (SD ≈ 0.2 Å). The highest deviations were located at the complex interface (residues 8−22 and 43−55) and were the result of optimization of packing interactions with cyt c.

DISCUSSION

In the work presented here, we sought to identify the surface of cyt b_5 that binds to cyt c. The use of proton NMR chemical shift analysis to characterize the binding surfaces in a protein complex between plastocyanin and cyt c has been demonstrated (*58*). The observed shift differences were small in the plastocyanin−cyt c complex and were interpreted as a dynamic ensemble of structures in fast exchange. For the cyt b_5−cyt c complex, the observed shift differences are also small, with our largest proton shift difference of 0.15 ppm, about three times as large as the largest shift differences observed for the plastocyanin−cyt c complex. Previous studies have shown that, for the ferric cyt b_5−ferric cyt c complex, the proteins are in fast exchange (*13*, *15*). In our NOESY spectra, we do not detect any cross-peaks between cyt b_5 and cyt c, suggesting that the complex is in fast exchange, and that the complex consists of a dynamic ensemble of structures. The static binary model of the cyt b_5−cyt c complex proposed by Salemme (*7*) has been used as the basis for subsequent studies of the interactions between cyt b_5 and cyt c; however, current opinion suggests that the

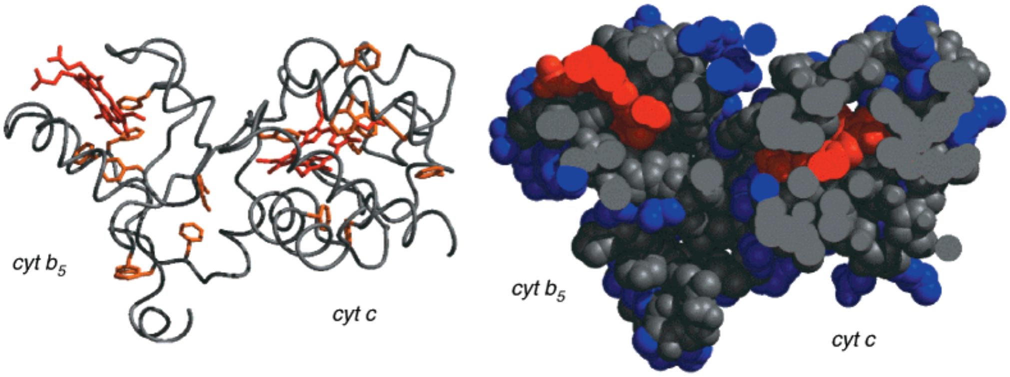

FIGURE 7: Final structure from the 2 ns simulation of the "cleft complex". The complex on the left shows how the path between the heme groups (in red) is lined by aromatic amino acids (in orange). The structure on the right is a space filling model of a slice through the same complex with the nonpolar residues colored gray and the polar in blue. The nonpolar path between the hemes suggests a potential electron-transfer route.

complex between cyt b_5 and cyt *c* can be better described as an ensemble of dynamic complexes (*3*, *59*). In this study, we sought to identify the binding site of these complex ensembles. To this end, heteronuclear NMR experiments were used to determine which residues on cyt b_5 were affected upon binding to cyt *c*.

Residues whose chemical shifts change upon binding cluster into two regions. The first is the anionic surface surrounding the heme where Salemme predicted cyt *c* would bind. (Figure 4). Previous NMR studies from this laboratory using pseudocontact shifts as restraints in the solution structure between cyt b_5 and cyt *c* provided direct experimental data that cyt *c* bound to cyt b_5 in the area predicted by Salemme (*1*). Indeed numerous other studies from a variety of investigators also support the existence of the Salemme complex (*60*, *61*, *9*, *3*).

The second region that experiences large chemical shift changes in the ferrous complex is the flexible loop region between residues 10−20 (*18*). It has been observed in other NMR studies of protein−protein interactions that complex formation can induce direct effects at the contact site as well as indirect effects due to small structural changes transmitted through the protein. These secondary changes frequently extend outside of the direct interaction surface (*62*, *63*, *58*). At present, the precise cause of the chemical shift changes observed here is unknown. There are several possible explanations for these chemical shift changes no one of which can be unambiguously demonstrated experimentally with the available data. The first possibility is that the binding of cyt *c* at the anionic surface of cyt b_5 induces conformational changes in one or more of the four α helices and β4 sheet comprising the hydrophobic heme binding pocket. The structurally perturbed β 4 sheet, beginning with residue 21, could subsequently propagate a conformational change to the adjacent loop between residues 10−20. The crystal structure of the Asn57Asp, Gln13Glu, Glu11Gln, triple mutant of cyt b_5, shows the largest difference between the mutant and wild-type protein in the vicinity of Ser18. The main-chain atoms of Ser18 have an average deviation of over 2 Å between the triple mutant and wild-type structure (64). The amino acid residues in the loop (10−20), which contains two type I turns (residues 12−15 and 17−20), also exhibit extensive hydrogen bonding to other amino acids in the loop. Thus, minimal structural changes in the loop might be propagated to other amino acids in the loop leading to large chemical shifts. Because of the small energies being monitored by NMR, a small conformational change can cause a relatively large chemical shift change. The second possible mechanism is that Salemme complex formation could induce dynamic changes in the loop region, perhaps altering the conformational mix of structures, from which we get a single averaged chemical shift for each resonance. There is no evidence, however, for such a mechanism from either the NMR experiments or the simulations. In the crystal structure of cyt b_5, the side chains and the backbone atoms of this loop possess the largest isotropic thermal parameters, or *B* factors, which reflect internal mobility among other factors (*55*).

A third mechanism by which the chemical shift changes in the loop region may occur is by the binding of cyt *c* in the cleft predicted to form when the loop moves, exposing the underlying heme. In a previous MD simulation of cyt b_5 (*18*), a large number of residues underwent cyclical conformational changes, which caused the protein to display different patterns of residues at the surface with time. The simulation also predicted that a large cleft partially exposing the hydrophobic core lining the heme pocket becomes transiently exposed. In that simulation study, the following residues were identified as the surface residues along the rim of the cleft: N16, N17, S18, K19, I24, T33, L36, E37, R47, A50, G51, and G52; interestingly, all of these residues displayed significant chemical shift changes ($\Delta\delta \approx 0.06$ Hz) upon binding cyt *c* in this study, except I24 (with $\Delta\delta \approx 0.05$ Hz) and G52. A number of residues (T21, L23, L32, L46, and A54) were calculated to become exposed to solvent only upon cleft formation in the simulation. With the exception of L46, these residues also undergo significant chemical shift changes upon complexation. However, alanine 54 also has minimal solvent exposure on the Salemme site. The molecular dynamics simulation of the cleft complex presented here suggests that such a complex is feasible. Of the 28 residues predicted to be near cyt *c* in the simulation of the cleft complex, 23 exhibited changes in chemical shift upon binding (Figure 4). Furthermore, there are experiments that also point toward the existence of a second binding site for cyt *c* on cyt b_5 (*10*, *65*, *15*, *14*). A "rolling ball" model for cyt b_5−cyt *c* interactions in which cyt *c* could roll along the surface of cyt b_5 between different binding modes has been proposed (*14*). In this regard, it is interesting to note that the Salemme and cleft binding surfaces are near in space and overlap at residues 48 and 49 (Figure 4).

The smaller complex-induced chemical shift differences observed in the ferric system suggest that binding could be weaker in the oxidized state. The weaker binding may reflect an increase in the dynamics of free and complexed ferric cyt b_5 and cyt *c* compared to their reduced counterparts. This suggestion is consistent with results from recent studies on the backbone dynamics of rat cyt b_5 and cyt *c* in the reduced and oxidized states (*66*, *67*) where the oxidized proteins were observed to be more flexible than the reduced form. So, aside from dynamic behavior affecting binding surfaces, as with the cleft, more subtle forms of mobility may also be important in recognition and regulation. For example, if cyt b_5 gains flexibility after transferring its electron to its redox partner, which then becomes more rigid upon reduction, then the dependence of a protein's flexibility on oxidation state might be a mechanism for modulating interactions with other proteins. Additional studies are underway which would confirm or refute a second binding site for cyt *c* on cyt b_5 under our experimental conditions.

ACKNOWLEDGMENT

UCSF MidasPlus was used to make Figures 4, 5, and 7 (*68*, *69*). Mass Spectrometry was provided by the Mass Spectrometry Facility (A.L. Burlingame, Director), University of California, San Francisco (supported by the Biomedical Research Technology Program of the National Center for Research Resources, NIH NIEHS ES04705 and NIH NCRR BRTP RR01614).

SUPPORTING INFORMATION AVAILABLE

Chemical shifts of the free and bound ferrous and ferric cyt b_5. This material is available free of charge via the Internet at http://pubs.acs.org.

REFERENCES

1. Guiles, R. D., Sarma, S., DiGate, R. J., Banville, D., Basus, V. J., Kuntz, I. D., and Waskell, L. (1996) *Nat. Struct. Biol. 3*, 333−339.
2. Wendoloski, J. J., Matthew, J. B., Weber, P. C., and Salemme, F. R. (1987) *Science 238*, 794−796.
3. Mauk, A. G., Mauk, M. R., Moore, G. R., and Northrup, S. H. (1995) *J. Bioenerg. Biomembr. 27*, 311−330.
4. Mathews, F. S., Levine, M., and Argos, P. (1972) *J. Mol. Biol. 64*, 449−464.
5. Dickerson, R. E., Takano, T., Eisenberg, D., Kallai, O. B., Samson, L., Cooper, A., and Margoliash, E. (1971) *J. Biol. Chem. 246*, 1511−1535.
6. Muskett, F. W., Kelly, G. P., and Whitford, D. (1996) *J. Mol. Biol. 250*, 172−189.
7. Salemme, F. R. (1976) *J. Mol. Biol. 10*, 563−568.
8. Eltis, L. D., Herbert, R. G., Barker, P. D., Mauk, A. G., and Northrup, S. H. (1991) *Biochemistry 30*, 3663−3674.
9. Northrup, S. H., Thomasson, K. A., Miller, C. M., Barker, P. D., Eltis, L. D., Guillemette, G., Inglis S. C., and Mauk, A. G. (1993) *Biochemistry 32*, 6613−6623.
10. Mauk, M. R., Reid, L. S., and Mauk, A. G. (1982) *Biochemistry 21*, 1843−1846.
11. Mauk, M. R., Mauk, A. G., Weber, P. C., and Matthew, J. B. (1986) *Biochemistry 25*, 7085−7091.
12. Mauk, M. R., Barker, P. D., and Mauk, A. G. (1991) *Biochemistry 30*, 9873−9881.
13. Eley, C. G., and Moore, G. R. (1983) *Biochem. J. 215*, 11−21.
14. Burch, A. M., Rigby, S. E., Funk, W. D., MacGillivray, R. T., Mauk, M. R., Mauk, A. G., and Moore, G. R. (1990) *Science 247*, 831−833.
15. Whitford, D., Concar, D. W., Veitch, N. C., and Williams, R. J. P. (1990) *Eur. J. Biochem. 192*, 715−721.
16. Moore, G. R., Cox, M. C., Crowe, D., Osborne, M., Rosell, F. I., Bujons, J., Barker, P. D., Mauk, M. R., and Mauk, A. G. (1998) *Biochem. J. 332*, 439−449.
17. Whitford, D., Gao, Y., Pielak, G. J., Williams, R. J., McLendon, G. L., and Sherman, F. (1991) *Eur. J. Biochem. 200*, 359−367.
18. Storch, E. M., and Daggett, V. (1995) *Biochemistry 34*, 9682−9693.
19. Sambrook, J., Fritsch, E. F., and Maniatis, T. (1989) *Molecular Cloning: A Laboratory Manual*, 2nd Edition, Cold Spring Harbor Laboratory Press, Plainview, NY.
20. Cristiano, R. J., and Steggles, A. J. (1989) *Nucleic Acid Res. 17*, 799−815.
21. Ikemura, T. (1985) *Mol. Biol. Evol. 2*, 13−34.
22. Reid, L. S., and Mauk A. G. (1982) *J. Am. Chem. Soc. 104*, 841−845.
23. Ozols, J., and Strittmatter, P. (1964) *J. Biol. Chem. 239*, 1018−1023.
24. Estabrook, R. W., and Werringloer, J. (1978**)** *Methods Enzymol. 52*, 212−220.
25. Altman, J., Lipka, J. J., Kuntz, I. D., and Waskell, L. (1989) *Biochemistry 28*, 7516−7523.
26. Davis, J. H. (1995) *J. Biol. NMR 5*, 433−437.
27. Kay, L. E., Keifer, P., and Saarinen, T. (1992) *J. Am. Chem. Soc. 11*, 10663−10665.
28. Yamazaki, T., Forman-Kay, J. D., and Kay, L. E. (1993) *J. Am. Chem. Soc. 115*, 11054−11055.
29. Zerbe, O., Szyperski, T., Ottiger, M., and Wüthrich, K. (1996) *J. Biol. NMR 6*, 99−106.
30. Muhandiram, D. R., and Kay, L. E. (1994) *J. Magn. Reson. 10*, 203-216.
31. Kay, L. E., Ikura, M., Tschudin, R., and Bax, A. (1990) *J. Magn. Reson. 8*, 496−514.
32. Grezsiek, S., and Bax, A. (1992) *J. Magn. Reson. 96*, 432−440.
33. Wittekind, M., and Mueller, L. (1993) *J. Magn. Reson. 101*, 201−205.
34. Grezsiek, S., and Bax, A (1992) *J. Am. Chem. Soc. 114*, 6291−6293.
35. Grzesiek, S., and Bax, A. (1993) *J. Biomol. NMR 3*, 185−204.
36. Bax, A., Clore, G. M., and Gronenborn, A. M. (1990) *J. Magn. Reson. 8*, 425−431.
37. Grezesiek, S., and Bax, A. (1993) *J. Magn. Reson. 10*, 103−106.
38. Brutscher, B., Simorre, J.-P., Caffrey, M. S., and Marion, D. (1994) *J. Magn. Reson. 105*, 77−82.
39. Marion, D., Ikura, M., Tschudin, R., and Bax, A. (1989) *J. Magn. Reson. 8*, 393−399.
40. Day, M. (1990) *Striker*, *NMR Processing Program*, unpublished, Copyright University of California, San Francisco.
41. Delaglio, F., Grzesiek, S., Vuister, G. W., Zhu, G., Peifer, J., and Bax, A. (1995) *J. Biol. NMR 6*, 277−293.
42. Kneller, D., and Kuntz, I. D. (1993) *Sparky, NMR Display and Analysis Program*, Copyright University of California, San Francisco.
43. Goddard, T., and James, T. L. (1997) *Sparky, NMR Display and Analysis Program, Version 3.3.2*, Copyright University of California, San Francisco.
44. Altieri, A. S., Hinton, D. P., and Byrd, R. A. (1995) *J. Am. Chem. Soc. 117*, 7566−7567.
45. Qi, P. X., Beckman, R. A., and Wand, A. J. (1996) *Biochemistry 35*, 12275−12286.
46. Levitt, M., Hirshberg, M., Sharon, R., and Daggett, V. (1995) *Comput. Phys. Commun. 91*, 215−231.
47. Levitt, M., Hirshberg, M., Sharon, R., Laidig, K. E., and Daggett, V. (1997) *J. Phys. Chem. B 101*, 5051−5061.

48. Henry, E. R., Levitt, M., and Eaton, W. A. (1985) *Proc. Natl. Acad. Sci. U.S.A. 82*, 2034−2038.
49. Kell, G. S. (1967) *J. Chem. Eng. Data 12*, 66−69.
50. Guiles, R. D., Basus, V. J., Sarma, S., Malpure, S., Fox, K. M., Kuntz, I. D., and Waskell, L. (1993) *Biochemistry 32*, 8329−8340.
51. Guiles, R. D., Altman, J., Kuntz, I. D., and Waskell, L. (1990) *Biochemistry 29*, 1276−1289.
52. Dangi, B., Sarma, S., Yan, C., Banville, D. L., and Guiles, R. D. (1998) *Biochemistry 37*, 8289−8302.
53. Keller, R. M., and Wüthrich, K. (1980) *Biochim. Biophys. Acta 621*, 204−217.
54. Slijper, M., Kaptein, R., and Boelens, R. (1996) *J. Magn. Reson. 111b*, 199−203.
55. Durley, R. C. E., and Mathews, F. S. (1996) *Acta Crystallogr. 52*, 65−76.
56. Storch, E. M., Daggett, V., and Atkins, W. M. (1999) *Biochemistry 38*, 5054−5064.
57. Storch, E. M., Grinstead, J. S., Campbell, A. P., Daggett, V., and Atkins, W. M. (1999) *Biochemistry 38*, 5065−5075.
58. Ubbink, M., and Bendall, D. S. (1997) *Biochemistry 36*, 6326−6335.
59. McLean, M. A., and Sligar, S. G. (1995) *Biochem. Biophys. Res. Commun. 215*, 316−320.
60. Rodgers, K. K., and Sligar, S. G. (1991) *J. Mol. Biol. 221*, 1453−1460.
61. Rodgers, K. K., Pochapsky, T. C., and Sligar, S. G. (1988) *Science 240*, 1657−1659.
62. Yi, Q., Erman, J. E., and Satterlee, J. D. (1994) *Biochemistry 33*, 12032−12041.
63. Wilde, J. A., Bolton, P. H., Dell'Acqua, M., Hibler, D. W., Pourmotabbed, T., and Gerlt, J. A. (1988) *Biochemistry 27*, 4127−4132.
64. Funk, W. D., Lo, T. P., Mauk, M. R., Brayer, G. D., MacGillivray, R. T. A., and Mauk, A. G. (1990) *Biochemistry 29*, 5500−5508.
65. Wilie, A., Stayton, P., Sligar, S. G., Durham, B., and Millett, F. (1992) *Biochemistry 31*, 7237−7242.
66. Dangi, B., Blankman, J., Miller, C. J., Volkman, B. F., and Guiles, R. D. (1998) *J. Phys. Chem. B. 102*, 8201−8208.
67. Banci, L., Bertini, I., Cavazza, C., Felli, I. C., and Koulougiotis, D. (1998), *Biochemistry 37*, 12320−12330.
68. Ferrin, T. E., Huang, C. C., Jarvis, L. E., and Langridge, R. (1988) *J. Mol. Graphics 6*, 13−27.
69. Huang, C. C., Petersen, E. F., Klein, T. E., Ferrin, T. E., and Langridge, R. (1991) *J. Mol. Graphics 9*, 230−236.

BI001129O